ECCOMAS Congress 2016
VII European Congress on Computational Methods in Applied Sciences and Engineering
M. Papadrakakis, V. Papadopoulos, G. Stefanou, V. Plevris (eds.)
Crete Island, Greece, 5–10 June 2016

PARTICLE BASED SIMULATION OF FLUID FLOW IN PERIODICALLY GROOVED CHANNELS

Dorothea Kasiteropoulou, Theodoros Karakasidis, and Antonios Liakopoulos

Hydromechanics and Environmental Engineering Laboratory,

School of Engineering University of Thessaly, 38334 Pedion Areos, Volos, Greece

dkasiter@uth.gr, thkarak@uth.gr, aliakop@uth.gr

Keywords: Dissipative Particle Dynamics, coarse-graining, fluid/wall interactions, protrusion size effect, friction factor, cut-off radius.

Abstract. *The method of Dissipative Particle Dynamics is applied to investigate the effect of the parameters employed to model the presence of periodic rectangular wall roughness on planar nanochannel flow. The parameters considered here include the fluid/wall interactions, the range of interaction of fluid particles and wall particles (cut-off radius), the external applied force and the coarse-graining parameter (number of atoms per DPD particle). Protrusions of upper wall are modeled by periodically spaced rectangular protruding elements. The dependence of flow pattern on protrusion length and the amplitude of these parameters is investigated. The computed macroscopic quantities of practical interest include density, velocity, and pressure fields. Fluid particle localization near the solid wall is affected by the conservative force and the cut-off radius. Fluid velocity reduces as the protrusion length decreases for constant parameters and reduces as both the conservative force and the cutoff radius increases. The pressure is uniform across most of the channel and their pattern near and inside the cavities depend on the protrusion shape, the conservative force and cut-off radius. For the coarse graining parameter, the density and pressure remain almost constant in the core of the channel and their pattern near and inside the cavities depends on the protrusion shape.*

1 INTRODUCTION

An adequate description of fluid flow over a solid boundary with surface roughness on multiple length scales often requires resolution of fine microscopic details on the flow structure while retaining peculiarities of a macroscopic picture [1]. Starting from the molecular/particle description, which is employed to model a small part of the computational domain where the continuum models fail to capture the physics of the system, there are many reports on wall structure, wall wettabillity and stiffness, the fluid-wall interface and also the combination of these parameters. For example, Davies et al. [2] investigated the laminar flow in a microchannel with superhydrophobic walls exhibiting transverse ribs and found that reductions in the friction factor and enhancements in the fluid slip are greater as the cavity-to-rib length ratio is increased (increasing shear-free fraction) and as the channel hydraulic diameter is decreased. Niavarani and Priezjev [3], investigated the combined effect of surface roughness and shear rate on slip flow of simple fluids by molecular dynamics simulation and found that in the region where the curved boundary faces the mainstream flow, the local slip is suppressed due to the increase in pressure. Kamali and Kharazmi [4] studied the surface roughness effects on the fluid flow in a nanochannel of simple fluids in hydrophobic and hydrophilic walls by molecular dynamic simulation. The simulation results show that the roughness and protrusions of the same dimensions induce different local density pattern while the overall average might be the same. Asproulis and Drikakis [5] investigated the effects of surface roughness on the flow behavior inside micro and nanofluidic devices. They found that as the surface attraction energy or the roughness height increase, the density layering near the wall is enhanced by higher values or secondary layering phenomena. Kasiteropoulou et al. [6] discussed the relation of friction factor, f, with the flow Reynolds number in a dissipative particle dynamics study of flow in periodically grooved nanochannels and found that the computed value for friction factor increases as the length decreases for the same Reynolds number. Sun et al. [7] investigated the effects of surface wettability and topology in the multi-scale liquid flow in micro/nanochannels.

Analysis on the flow friction shows that the pressure gradient decreases in a power law with increasing channel height. The confinement on the liquid molecules will equivalently narrow the channel, where larger pressure gradient is needed to keep the flow conditions from changing. The larger the roughness is, the more obvious the influence will be. When the channel height becomes larger, both velocity slip and relative slip length will gradually converge to 0, which means that different flow boundaries will be unified to be non-slip at conventional spatial scale. Priezjev [8] reported the results obtained from Molecular Dynamic simulations of the friction at an interface between polymer melts and weakly attractive crystalline surfaces. He found that the friction coefficient at small slip velocities exhibits a distinct maximum which appears due to shear – induced alignment of semiflexible chain segments in contact with solid walls and at large slip velocities, the friction coefficient is independent of the chain stiffness. Later, Chen et al. [9] estimated the velocity slip on curved surfaces in a Couette flow studied by molecular dynamics simulation. They found that the slip length as conventionally measured at a flat wall in Couette flow is the same as that for all other cases with curved and rotating boundaries, provided the atomic interactions are the same and boundary shape is properly taken into account. Priezjev [10] investigated the effect of interfacial slip on steady-state and time-periodic flows of monatomic liquids by using non-equilibrium molecular dynamics simulations. They found that the velocity profiles in oscillatory flows are well described by the Stokes flow solution with the slip length that depends on the local shear rate. For both types of flows, the friction coefficient at the liquid–solid interface correlates well with the structure of the first fluid layer near the solid wall.

Sofos et al. [11] studied the wetability and stiffness on diffusion in grooved nanochannel and observed a significant anisotropy along the directions parallel and normal to the flow inside the grooves.

On the other hand, at macroscale description slip or wettabillity parameters are not usually performed in numerical simulations whereas the surface construction, such as the protruding elements mentioned above, seem to concern the scientific community for many years. We report here some examples of these investigations. Sahan et al. [12] investigated the two-dimensional isothermal flow in a periodically grooved channel. They presented low-order models successfully which describe the dynamical characteristics of the flow for Re close to the design conditions. They found that far from the design conditions, the reduced models predict quasi-periodic or period-doubling routes to chaos as Re is increased [13]. Greiner et al. [14] investigated the three-dimensional flow in a channel with symmetric, transverse grooves on two opposite walls by using the spectral element technique. They observed the transition from steady two- dimensional flow in the three-dimensional mixing through two and three dimensional wave structures as the Reynolds number was increased. Chung et al. [15] studied the unsteady laminar flow in grooved channel and also in a sharp 180^o bend for low Reynolds number. This model is used in the cooling of high performance modern electronic systems [16]. Adachi & Hasegawa [17] investigated the flow influence of the number of grooves in which the flow repeats periodically. Above these, flows around and inside grooves at the larger dimensions can also present some other interesting dynamic flow phenomena. In particular, when the flow increases its speed can experience shock waves and shock/vortex interactions. Large eddy simulations can be used for understanding such phenomena [18, 19] and can also be combined with MD [20, 21] to shed light on scale-up effects.

In the present work we study the flow in a nanochannel of height 4.72nm and seek further insight on the effects of wall protrusions and parameters inserted on the system on the flow rate based on mesoscopic Dissipative Particle Dynamics simulations. Protrusions are introduced by periodically placing rectangular protruding elements on one of the two channel walls. Pressure, density and velocity profiles are calculated for different protrusion lengths. Protrusion size, fluid-wall interaction, cut-off radius and coarse-graining parameter plays an important role on flow properties such as density, velocity and pressure distributions.

We remind here the reader that in the nanochannel cases the coarse graining parameter is equal to 1 (an atom per DPD particle) while in the microchannel cases is $2.5x10^6$. The corresponding heights are set equal to 4.72 nm for the nanochannel and 1.1μm for the microchannel.

This paper is set up as follows. Section 2, gives a description of the system and the simulation method. In Section 3 the results are shown and analyzed, whereas section 4 contains concluding remarks.

2 SIMULATION METHOD

2.1 Channel Geometry

We study pressure-driven (or body-force driven) flow between two parallel walls. The lower wall is flat whereas the upper wall consists of protrusions modeled by rectangular elements (see Fig. 1). We considered protrusions of three length values and one height at the upper wall: $l_{r_1}=0.5l_{tot}$, $l_{r_2}=0.25l_{tot}$, $l_{r_3}=0.125l_{tot}$ *or* $l_{r_3}=0.167l_{tot}$ for the microchannel case (protrusion length) and h=0.10H *or* h=0.125 $\bar{h}$ (protrusion height), where l_{ri} and h represent the length

and the height of the rectangular grooves on the upper wall and $l_{tot,}$ H represent the length of the computational domain along the x-direction and it's height in the y-direction respectively and $\bar{h}$ represents the distance between the solid walls. Therefore case $l_{r1}=0.5l_{tot}$ corresponds to a computational domain with one rectangular groove, $l_{r2} = 0.25l_{tot}$ corresponds to two rectangular grooves, and $l_{r3} = 0.125l_{tot}$/ $l_{r3}=0.167l_{tot}$ corresponds to three/four rectangular grooves. Baseline dimensions of all computational domains in x-, y- and z-directions are 3.77nm x 4.72nm x 3.77nm for the nano- and L_x x L_y x L_z = 1.11 μm x 1.3μm x 1.1 μm for the microchannel (in DPD units the dimensions are L_x x L_y x L_z = 11.09 r_c x 13.87 r_c x 11.09 r_c and 11.14 r_c 13.00 r_c x 11.14 r_c respectively). Conversion from DPD units to physical units is discussed in detail in Kumar et al. [32].

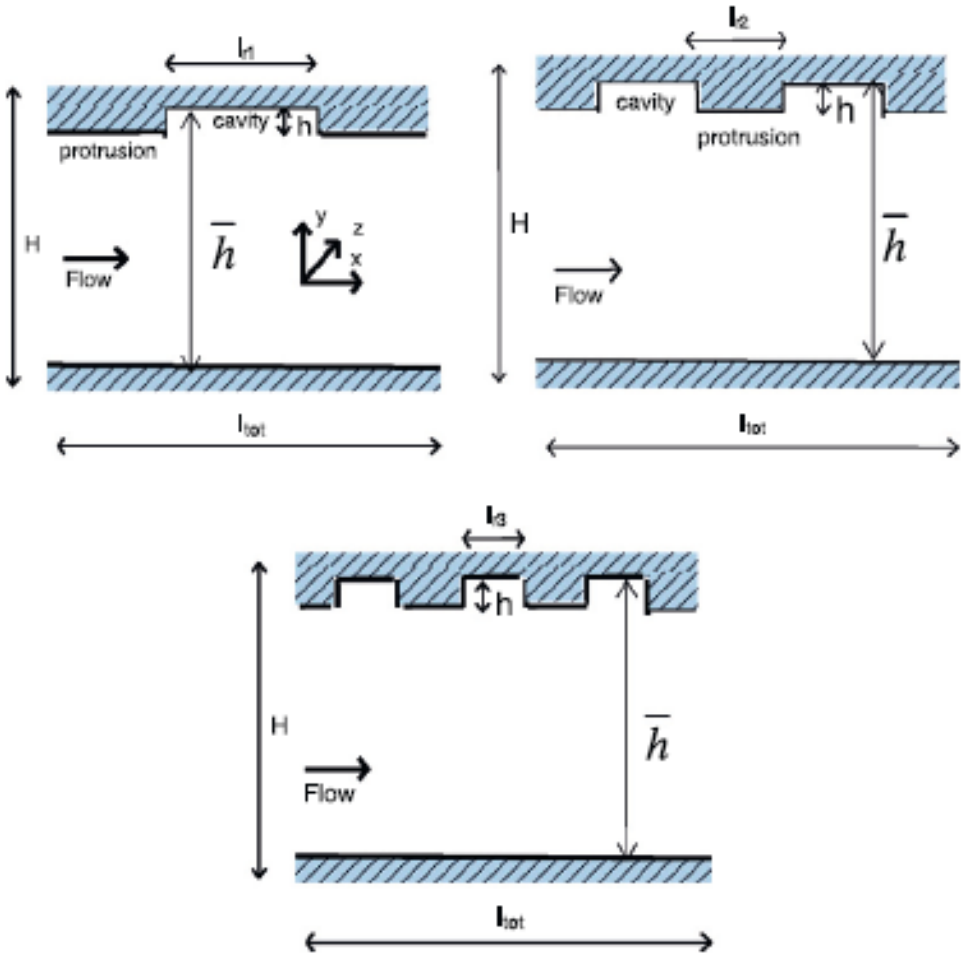

Fig. 1. Schematics of computational domains (adapted from Kasiteropoulou et al. [35]).

2.2 Mathematical Model and Computational details

2.2.1. Dissipative Particle Dynamics

The DPD system consists of N particles. For the i-th particle we denote mass m_i, position $\mathbf{r}_i$ and velocity $\boldsymbol{\upsilon}_i$, i=1,2,…N. For a single-component DPD liquid the forces exerted on a particle i due to particle j consists of three terms: 1) the conservative force $\mathbf{F}_{ij}^{C}$, 2) the dissipative force $\mathbf{F}_{ij}^{D}$ and 3) a random force $\mathbf{F}_{ij}^{R}$, given by,

$$\mathbf{F}_{ij}^{C}\left(r_{ij}\right)=\begin{cases}\alpha_{ij}\left(1-r_{ij}/r_c\right)\hat{\mathbf{r}}_{ij}, & for \quad r_{ij} \le r_c \\ 0, & for \quad r_{ij} > r_c\end{cases} \tag{1}$$

$$\mathbf{F}_{ij}^{D}=-\gamma\omega^{D}(r_{ij})(\mathbf{\upsilon}_{ij}\cdot\hat{\mathbf{r}}_{ij})\hat{\mathbf{r}}_{ij} \tag{2}$$

$$\mathbf{F}_{ij}^{R}=\sigma\omega^{R}(r_{ij})\xi_{ij}\hat{\mathbf{r}}_{ij} \tag{3}$$

where $\mathbf{r}_{ij}=\mathbf{r}_i-\mathbf{r}_j$, $r_{ij}=\left|\mathbf{r}_{ij}\right|$, $\hat{\mathbf{r}}_{ij}=\dfrac{\mathbf{r}_{ij}}{\left|\mathbf{r}_{ij}\right|}$, $\mathbf{\upsilon}_{ij}=\mathbf{\upsilon}_i-\mathbf{\upsilon}_j$ [22] and α_{ij} is the maximum repulsion between particles i and j [23]. The coefficients γ and σ determine the amplitude of the dissipative and random forces, respectively, while ω^D and ω^R are appropriate weight functions [24]. The weight functions ω^D and ω^R provide the range of interaction for the dissipative and random forces [25]. In Eq. (3), ξ_{ij} is a random variable with Gaussian statistics [23]. By enforcing $\xi_{ij}=\xi_{ji}$ one satisfies the principle of momentum conservation [26]. All the forces between particle i and j vanish beyond a cut-off radius r_c [27]. The random force coefficient, σ, the system temperature and the simulation timestep is the same for all cases studied here and their value was chosen following the methodology proposed by Groot and Warren [23].

The requirement of canonical distribution sets two conditions linking the random and dissipative forces. The first one couples the weight functions through

$$\omega^{D}\left(r_{ij}\right)=\left[\omega^{R}\left(r_{ij}\right)\right]^2 \tag{4}$$

and the second one the strengths of the random and dissipative forces via

$$\sigma^2=2\gamma k_B T \tag{5}$$

where k_B is the Boltzmann constant [27]. The typical choice for the weight functions is

$$\omega^{R}\left(r_{ij}\right)=\begin{cases}\left(1-r_{ij}/r_c\right)^{p}, & for \quad r_{ij} \le r_c \\ 0, & for \quad r_{ij} > r_c\end{cases} \tag{6}$$

where $p=1$, for the standard DPD method [28].

The time evolution of velocities and positions of particles are described by the following equations [29]

$$d\mathbf{r}_i=\mathbf{\upsilon}_i dt \tag{7}$$

$$d\mathbf{\upsilon}_i=\frac{1}{m}\left(\mathbf{F}_i^{C}dt+\mathbf{F}_i^{D}dt+\mathbf{F}_i^{R}\sqrt{dt}\right) \tag{8}$$

where $\mathbf{F}_i^{C}=\sum_{i\neq j}\mathbf{F}_{ij}^{C}$, and $\mathbf{F}_i^{R}=\sum_{i\neq j}\mathbf{F}_{ij}^{R}$.

All simulations are conducted using the open source LAMMPS package [30]. We use different values for the parameter a_{ij} when we describe fluid–fluid interactions, wall–wall interactions and wall–fluid interactions: a_{ww} for wall–wall interactions, a_{wf} for wall–fluid interaction, a_{ff} for fluid–fluid interactions. In our simulations we have kept the fluid–fluid parameter interaction constant: a_{ff} = 25 for N_m=1 and a_{ff} = 7.5 for N_m=2.5x10^6. The value of parameter a_{ij} has been selected so that the dimensionless compressibility of the simulated DPD fluid corresponds to a typical liquid, such as water both in the nanochannel and the

microchannel case studied (for the calculation of compressibility see [23]). This value of a_{ij} is employed in fluid–fluid interactions. We remind the reader that the cross interaction term obeys the relation $\alpha_{wf}=(\alpha_{ww}\ \alpha_{ff})^{1/2}$ (see for example Pivkin and Karniadakis [29]). The type of the surface (hydrophilic or hydrophobic) is controlled via the fluid–wall interaction through the conservative force parameter a_{ij} (Equation (1)), specifically by choosing appropriately the ratio of the a_{ij} parameters for the fluid–wall interaction versus a_{ij} parameters for fluid–fluid interactions [31]. The number density of the DPD fluid, n_f, is equal to 3 for the nanochannel case and 10 for the microchannel while the random and dissipative forces, σ and γ respectively, are set equal to those described in Pivkin and Karniadakis [29]. System temperature is kept constant at T*=1 (in real units the system temperature is equal to 300K).
In this work we investigated all the parameters inserted on a DPD system along with grooved channels. In the first place we employed a_{ff} = 25 and a_{wf} = 25 with r_c = 1.0 for the cut-off radius for particle interactions (equal to 1.0σ for the nanochannel, where σ denotes the characteristic length scale of the Lennard-Jones potential (0,3402nm) and not the force parameter of Eq.5) and N_m=1 (one atom per DPD particle – nanochannel case) and we examined the effect of the magnitude of the externally applied force by assigning four values (F_{ext} = 0.01, 0.02, 0.03, 0.04 DPD units). The external driving force is applied on each particle along the x-direction to drive the flow.
In the rest of the simulations F_{ext} = 0.02 DPD units was used. For the case $a_{ff} = a_{wf}$ = 25 and N_m=1 we explored the effect of range of interactions of DPD particles (cut-off distance) rc = 1.0σ, 1.5σ and 2.0σ. Keeping fixed the cut-off distance r_c = 1.0σ and N_m=1 we varied the values of wall–fluid interaction a_{wf} using three values of the conservative force parameter equal to a_{wf} = 25, 100, 200. Finally we changed the number of atoms per DPD particle equal to $2.5\text{x}10^6$ (microchannel case) atoms per particle, along with the particle interactions coefficient: $a_{ff} = a_{wf} = a_{ww}$ = 7.5 and rc = 1.0σ. In the last case F_{ext} = 0.02 DPD units was also used. By changing the cut-off distance we fix the fluid type. The wall material is controlled via the fluid-wall interaction.

Periodic boundary conditions are employed along x- and z-directions. Appropriate boundary conditions need to be enforced in order to avoid that fluid particles cross the wall, since the effective forces are not sufficient to prevent wall penetration and several models have been employed and tested to impose various boundary conditions, such as specular, Maxwellian and bounce back [29-33]. In general, according to the boundary conditions employed we may observe fluctuations, near the solid walls, in the density, velocity or temperature which in cases of modeling microscopic systems may be inconsistent with continuum models. Such variations are also observed in cases of nanochannels studied with Dissipative Particle Dynamics simulations [see for example 6, 31].
In the present study we have chosen to employ the bounce back conditions, in which both components of the velocity are reversed [33]. Wall particles are bound on sites of a cubic lattice and their velocities are set equal to zero.

The simulation timestep is $\Delta t = 0.01\sqrt{mr_c^2/k_BT}$ (0.015ps for the nanochannel and $7.6\text{x}10^{-3}$μs for the microchannel in physical units). The duration of each simulation is $5\text{x}10^5$ time steps. Pressure, number density, temperature and streaming velocity bin values are averaged over the last $2.5\text{x}10^5$ time steps of the simulation.

2.3 Macroscopic property evaluations

Local macroscopic property values are calculated in parallelepiped bins. Results presented in this work are obtained by dividing the computational domain into 4x80x80, 8x80x80, 16x80x80 bins along the direction x, y, z respectively for post processing. To extract average profiles (for pressure, density, velocity), mean values over space are computed at each layer along the channel for each time step, and these values are then averaged over time.

Pressure values are obtained from the trace of the stress tensor

$$p = -\frac{1}{3} tr\mathbf{S} \tag{9}$$

where the stress tensor, $\mathbf{S}$, is calculated using the Irving– Kirkwood theory [34,35]:

$$\mathbf{S} = -\frac{1}{V}\left[m\sum_i (\boldsymbol{\upsilon}_i - \boldsymbol{\upsilon})(\boldsymbol{\upsilon}_i - \boldsymbol{\upsilon}) + \frac{1}{2}\sum_i \sum_{j\neq i} \mathbf{r}_{ij}\mathbf{F}_{ij} \right] \tag{10}$$

where V is the volume of the computational bin, $\boldsymbol{\upsilon}$ is the corresponding stream velocity and $\mathbf{F}_{ij}$ is the interparticle force on particle i due to particle j:

$$\mathbf{F}_{ij} = \mathbf{F}_{ij}^{C} + \mathbf{F}_{ij}^{D} + \mathbf{F}_{ij}^{R} \tag{11}$$

3 RESULTS AND DISCUSSION

3.1 Nano-channel results: number density, flow velocity and pressure

In this section we present results concerning the variation of fluid number density (particle localization), velocity and pressure as a function of variation of fluid/wall interaction, the range of particle interactions (variation of cut-off radius) as well as the effect of the driving force.

3.1.1. Particle localization

The average number density profiles as a function of the fluid/wall interaction are presented in Fig. 2a for a typical protrusion length. We observe that as the conservative force increases the number density inside the cavities and near the walls become higher and more distant from the wall, a behavior which is called layering (for a more detailed description see Kasiteropoulou et al. [31]). This behavior is in qualitative agreement with the results of Sofos et al. [36] who investigated the surface wettability effects on flow in rough nanochannels and found that as the wall hydrophobicity decreases there is a kind of increased fluid atom localization. Actually we observe that the wall surface behaves more like a hydrophobic one as the conservative force parameter increases. In the lower flat wall the number density is higher for all cases studied here than the number density at the upper wall and this could be explained by the presence of the wall protrusions.

Number density profiles as a function of the distance of the particle interactions (cut-off distance) are presented in Fig.2b. As we can see the number of peak density inside the cavity regions depend on the cut-off distance. In fact, for cut-off distance r_c=2.0σ there are two number density peaks which are decreased as the cut-off distance decreases. Moreover we observe that near the lower and protrusion wall the increased range of interactions results in more important layering effect and density variations extending over larger distances. This behavior is in general detected in all the protrusion length investigated in this work and this

means that the fluid is less homogeneous as the range of interactions increases.

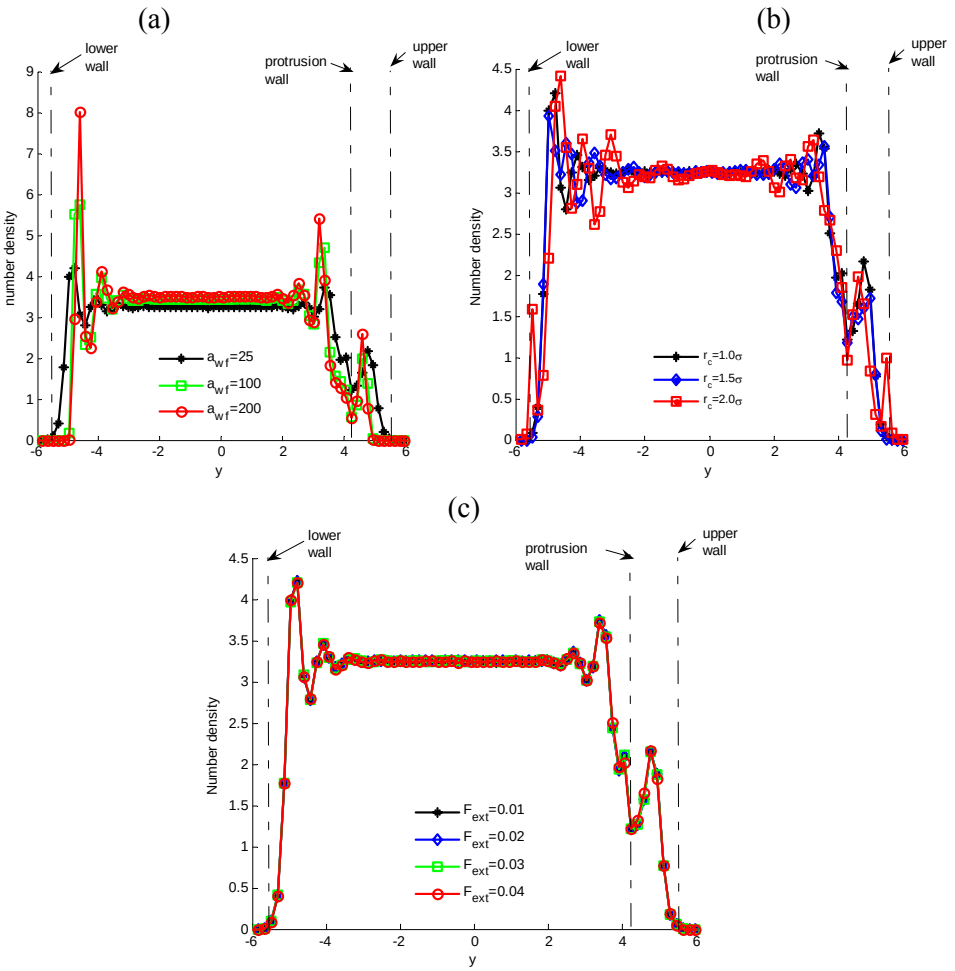

Fig. 2. Average number density profiles for $l_{r3}=0.125l_{tot}$ obtained by varying (a) wall–fluid interactions, a_{wf} (parameters kept constant: the cut-off radius $r_c = 1.0\sigma$, external driving force $F_{ext} = 0.02$, $a_{ff} = 25$), (b) the cut-off radius, r_c (parameters kept constant $a_{ff} = a_{wf} = 25$, and $F_{ext} = 0.02$), (c) the external driving force, F_{ext} (parameters kept constant $a_{ff} = a_{wf} = 25$, and $r_c = 1.0\sigma$). N_m=1. Dash-dot lines denote solid wall limits and y is in r_c units.

The external driving force seems to have no effect on the fluid particle localization (Fig. 2c) for all grooved channels, at least for the force range examined in the present work. Similar results are also reported by Young et al. [37] who reported that for a given surface wettability the fluid densities are independent of the driving force in a nanochannel flow.

The influence of the protrusion length for constant conservative force parameter is presented in Fig.3. We observe that number density inside the cavities and near the protrusion walls are reduced as the protrusion length decreases.

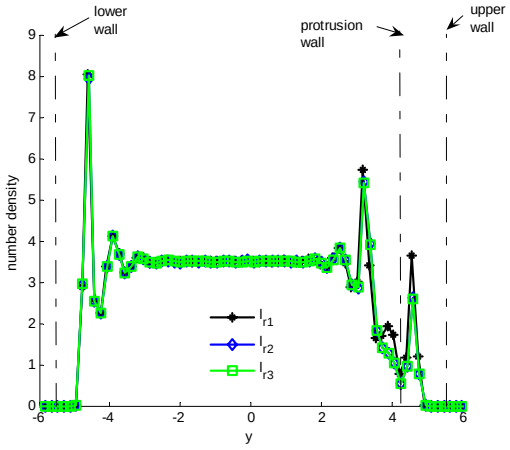

Fig. 3 Average number density profiles for a) $l_{r1}=0.5l_{tot}$, b) $l_{r2}=0.25l_{tot}$, c) $l_{r3}=0.125l_{tot}$ obtained by parameters a_{wf} = 200, a_{ff} = 25, r_c = 1.0σ and F_{ext} = 0.02. N_m=1. Dash-dot lines denote solid wall limits and y is in r_c units.

3.1.2. Flow velocity

The average velocity as a function of the conservative force parameter is presented in Fig. 4a. We observe that in the main core of the channel the flow velocity increases significantly as the fluid/wall interaction also increases and this behavior is also presented in the work of Sofos et al [36]. This behavior can be explained by the equations (1) and (8). As the conservative force parameter increases the total conservative force also increases (equation (1)) and this leads in higher velocity values (according to equation (8)).

(a) (b)

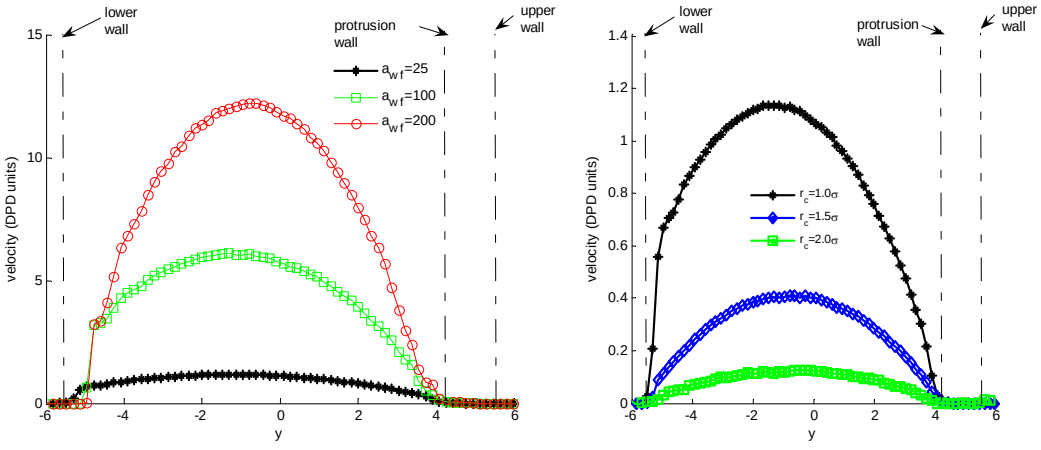

(c)

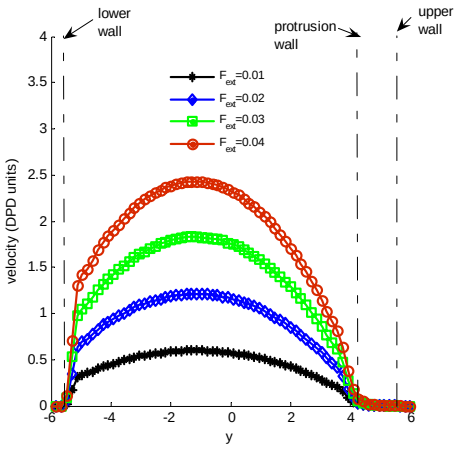

Fig. 4. Average velocity profiles for l_{r2}=0. 25l_{tot} obtained by varying (a) wall–fluid interactions, a_{wf} (parameters kept constant: the cut-off radius r_c = 1.0σ, external driving force F_{ext} = 0.02, a_{ff} = 25), (b) the cut-off radius, r_c (parameters kept constant a_{ff} = a_{wf} = 25, and F_{ext} = 0.02), (c) the external driving force, F_{ext} (parameters kept constant a_{ff} = a_{wf} = 25, and r_c = 1.0σ). N_m=1. Dash-dot lines denote solid wall limits and y is in r_c units.

As far as the range of interaction of the fluid and the wall particles (cut-off distance) concerned, we observe that the average velocity (Fig. 4b) is decreased as the cut-off radius increases.

The average velocity increases systematically as the external driving force increases (Fig. 4c). These results are in qualitative agreement with the results of Priezjev [38] where the effect of surface roughness on rate-dependent slip in simple fluids has been investigated.

3.1.3. Pressure profiles

The pressure profiles of all channel cases are presented in Fig.5 as a function of all the parameters investigated in this work. For all these parameters the pressure increases both inside the cavities and in the core of the channel as the parameters' value increases. The higher values of pressure are detected in the case of the cut-off distance increment (r_c=2.0σ) and also in the higher conservative force value (a_{wf}=200). In fact the pressure increases as the range of interaction increases among fluid as well as the fluid and wall particles. On the other hand, the conservative force parameter increases between the fluid and wall particles and this leads in higher conservative total force (according to Eq.6 and 10) and though higher pressure (according to Eq. 10). The pressure profile for various external driving force magnitudes is presented in Fig. 5c. Both in the core of the channel and inside the cavities the pressure peaks are detected in the same location for all external driving force magnitudes. The pressure increases systematically as the driving force increases but this behavior is of small interest relative to the other parameters described above.

The variation of protrusion lengths reveals some interesting characteristics. The isobars for constant conservative force parameter, equal to a_{wf}=25, are presented in Fig. 6. For case l_{r1} (Figure 6(a)), pressure reduces inside the cavities adjacent to the upper wall. However, there is a region of high pressure inside the cavities surrounded by two regions of low pressure. We believe that such high-pressure regions are observed because of the trapping of the fluid particles inside the cavities and the increased localization, as described is Section 3.1.1 (see also Figure 2(a)) [6]. This behavior results in smaller interparticle distances and thus higher interparticle forces leading to an increase of pressure. Adjacent to the protrusion wall, pressure is reduced, especially for smaller protrusion lengths, because particles are not localized there. For cases l_{r2} and l_{r3} (Figure 6(b) and 6(c)), at the rough wall, inside the

cavities, we observe that the shape of high-pressure regions depend on the protrusion length. More specifically, as the protrusion length decreases the length of the high pressure region increases.

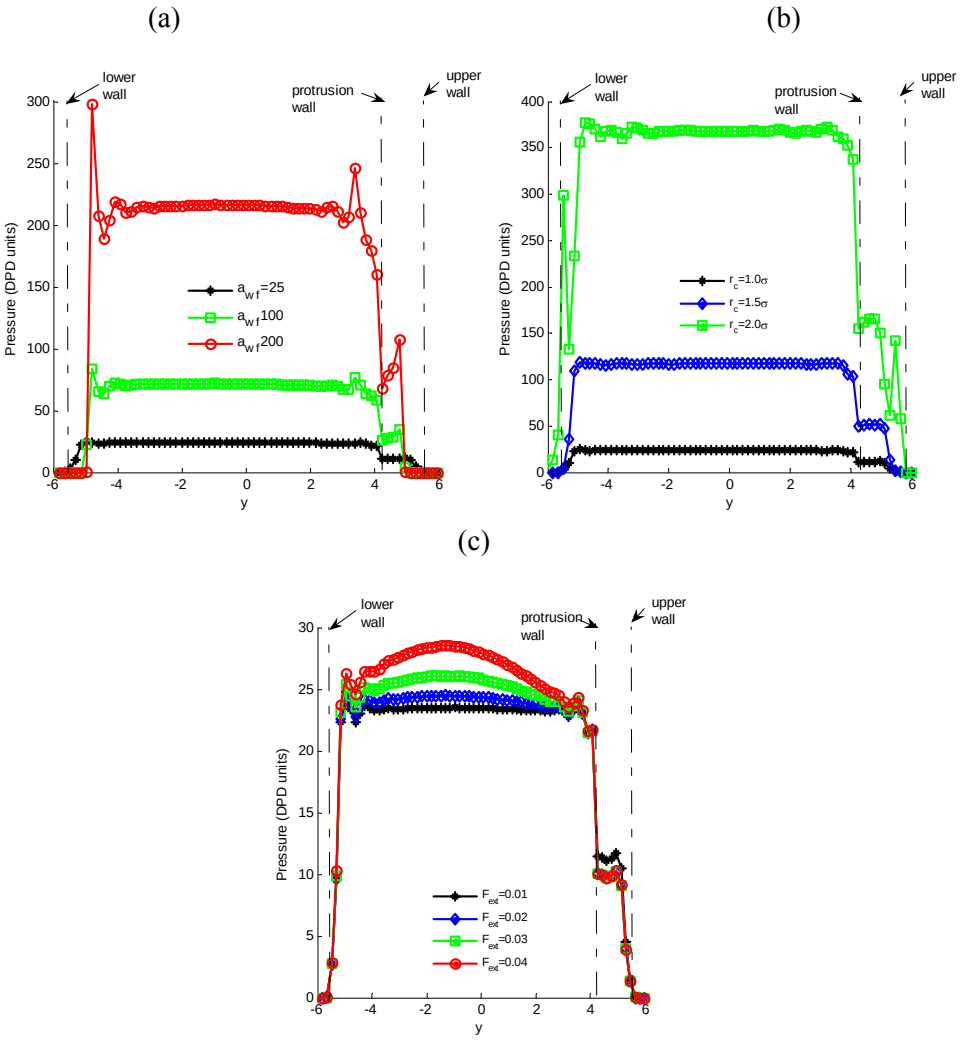

Fig. 5. Average pressure profiles for l_{r3}=0. 125l_{tot} obtained by varying (a) wall–fluid interactions, a_{wf} (parameters kept constant: the cut-off radius r_c = 1.0σ, external driving force F_{ext} = 0.02, a_{ff} = 25), (b) the cut-off radius, r_c (parameters kept constant a_{ff} = a_{wf} = 25, and F_{ext} = 0.02), (c) the external driving force, F_{ext} (parameters kept constant a_{ff} = a_{wf} = 25, and r_c = 1.0σ). N_m=1. Dash-dot lines denote solid wall limits and y is in r_c units.

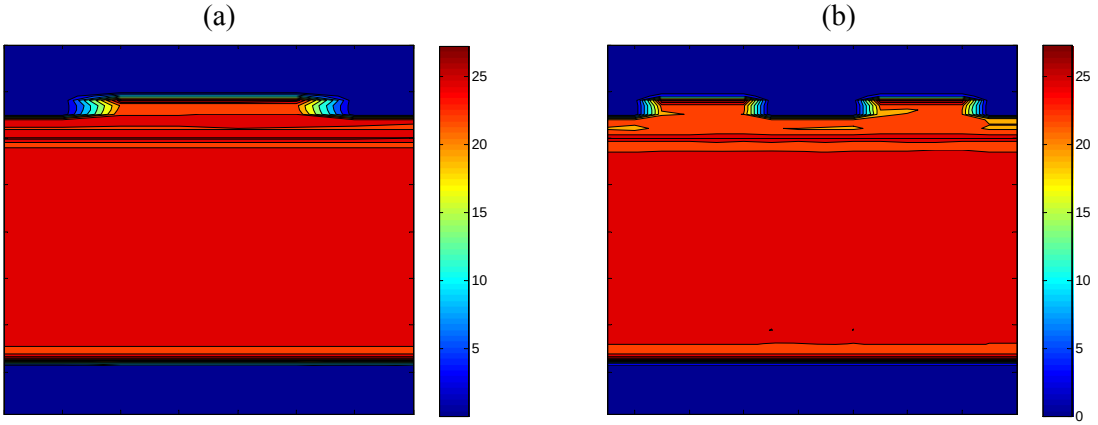

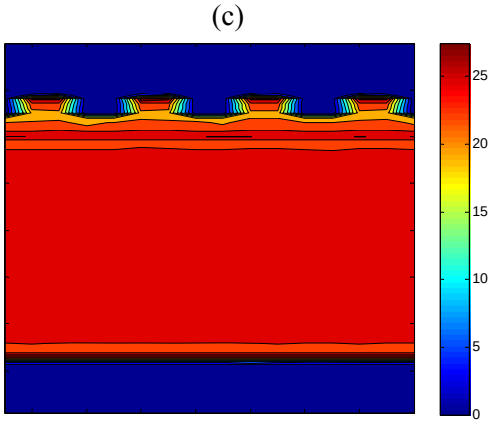

Fig. 6 Isobars for a) $l_{r1}=0.5l_{tot}$, b) $l_{r2}=0.25l_{tot}$, c) $l_{r3}=0.125l_{tot}$ obtained by parameters $a_{wf} = 25$, $a_{ff} = 25$, $r_c = 1.0\sigma$ and $F_{ext} = 0.02$. $N_m=1$. Dash-dot lines denote solid wall limits and y is in r_c units.

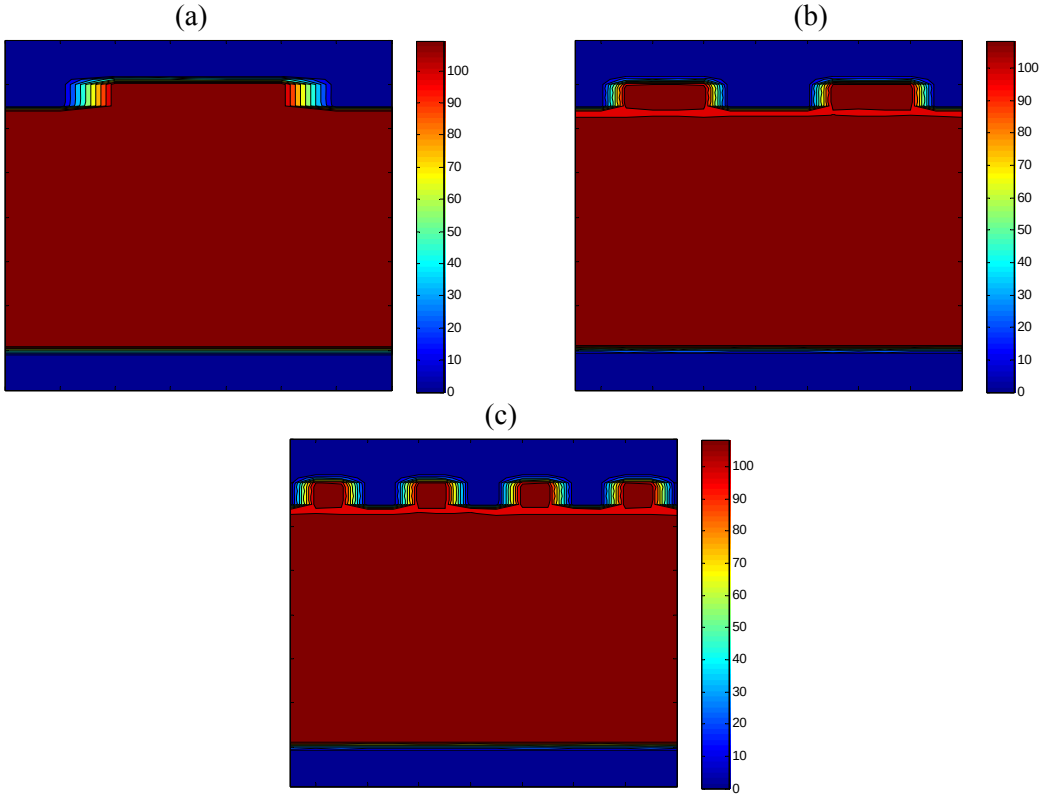

Fig. 7 Isobars for a) $l_{r1}=0.5l_{tot}$, b) $l_{r2}=0.25l_{tot}$, c) $l_{r3}=0.125l_{tot}$ obtained by parameters $a_{wf} = 25$, $a_{ff} = 25$, $r_c = 1.5\sigma$ and $F_{ext} = 0.02$. $N_m=1$. Dash-dot lines denote solid wall limits and y is in r_c units.

The isobars for constant cut-off distance equal to $r_c=1.5\sigma$ are presented in Fig. 7. Again, the pressure inside the cavities depends on the protrusion length. Although both inside and in the core of the channel the pressure is equal for the three protrusion lengths within statistical error, the distribution of the pressure inside the cavities is affected by the length. More thoroughly, for protrusion length equal to l_{r1} the high pressure region length exceeds all the protrusion height, whereas this height decreases slightly as the protrusion length decreases (see Figs. 7b and 7c for cases l_{r2} and l_{r3} respectively). Figure 7 reveal that the protrusion shape has small influence in the pressure map for constant cut-off distance.

3.2 Micro-channel results: number density, flow velocity, velocity slip, pressure and temperature

In this section we present results concerning the variation of fluid number density (particle localization), velocity and pressure as a function of the coarse-graining parameter by keeping constant the external driving force and the 'dimensionless' cut-off distance. By changing the coarse-graining parameter from value 1.0 to value $2.5x10^6$ we move through the scale of the channel and actually we "reach" the microscale dimension in our simulations.

3.2.1. Particle localization

Number density profiles at the protrusion and the cavity midplanes for the microchannel case are presented in Fig. 8. Fluid particle localization is similar for the nanochannel (Fig 2), and the microchannel case with peaks located at a distance from the walls ($0.87r_c$ and $0.44r_c$ for the nanochannel and the microchannel case respectively) for the same external driving force (F_{ext}=0.02 DPD units) and the same "dimensionless" cut-off distance (r_c=1.0). For the nanochannel case, at the protrusion midplanes density is homogeneous and slightly lower than its average value in the core of the channel while at the cavity midplanes is slightly higher (for the nanochannel case see also Fig.2 from Kasiteropoulou et al. [6]).

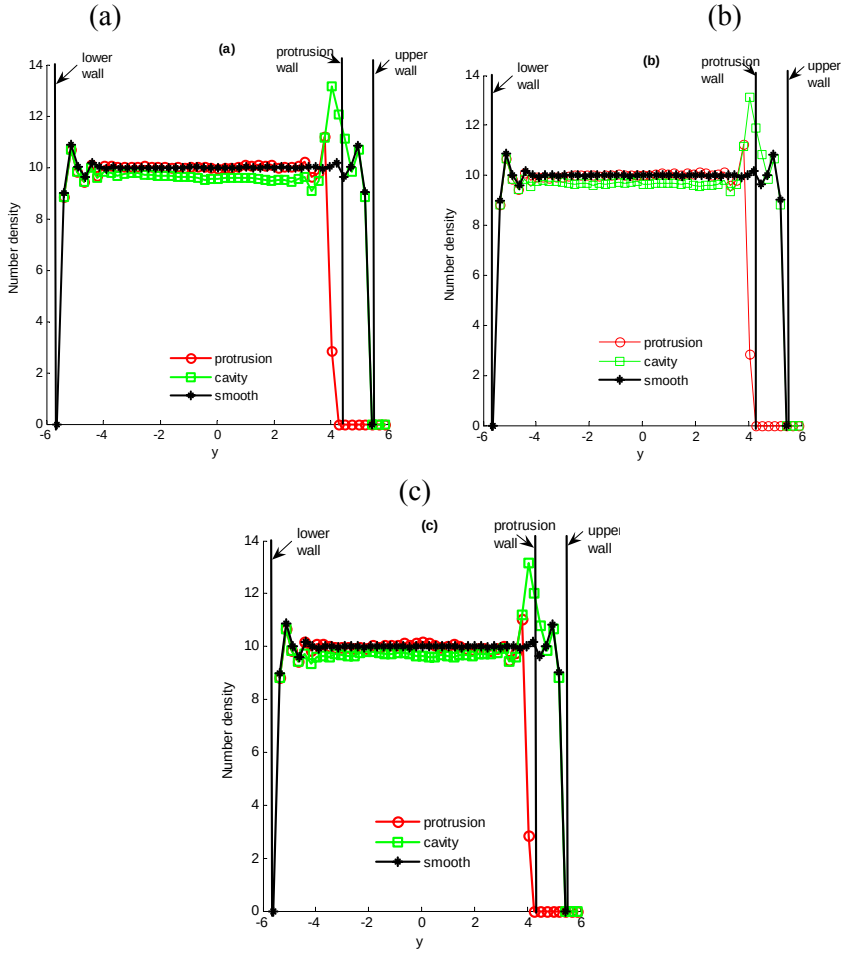

Fig. 8. Local number density profiles at the protrusion midpoints and the cavity midpoints obtained for $N_m=2.5x10^6$ and $a_{wf} = a_{ff} = a_{ww} = 7.5$ (parameters kept constant: the cut-off radius $r_c = 1.0$ and the external driving force $F_{ext} = 0.02$) for cases a) $l_{r1}=0.5l_{tot}$, b) $l_{r2}=0.25l_{tot}$, c) $l_{r3}=0.167l_{tot}$. Dash-dot lines denote solid wall limits and y is in r_c units.

In the microchannel case, at the protrusion midplanes density is almost equal to its average value in the core of the channel within statistical errors, while at the cavity midplanes density is lower. It should be also noted that in the microchannel case a high density peak is detected in the density profile very close to the protrusion surface ($y \approx 4.00 r_c$). Inside the cavities high number density regions are detected for both channel scales and suggest the possibility of particle trapping in these regions. Particle trapping is confirmed by computing the particle residence time and by the analysis of particle trajectories and is discussed in detail in Kasiteropoulou et al. [6] (nanochannel) and in Kasiteropoulou et al. [39] (microchannel).

Regarding the density fluctuations close to the solid walls, we must make some comments already discussed in [40]. For the nanoscale simulations using DPD, these oscillations are realistic. However, as the DPD particles get larger in size (the case of mesoscale simulations), these oscillations close to the wall extend over larger regions than those corresponding to physical layering zones as discussed in [41–43]. There are several methods that have been developed in order to limit such oscillations [41–43]. Thus, the observed oscillations in the mesoscale case have to be seen with some caution. Of course we must mention that if one wants to represent in detail the situation close to the wall, it is crucial to implement the above-mentioned methods. However, in our case, we are interested mostly on the qualitative flow behavior as a function of the protrusion shape and the parameters inserted on a DPD system and not to a detailed quantitative study. In a future study, it would be of interest to implement such methods and compare their results as far as the mesoscale is concerned.

An example of implementing these methods is discussed in [43]. Li et al.[43] in order to capture the correct temperature-dependence of a fluid, developed an energy-conserving dissipative particle dynamics (eDPD) model by expressing the weighting terms of the dissipative force and the random force as functions of temperature. They found that for non-isothermal fluid systems, the present model can predict the diffusivity and viscosity consistent with available experimental data of liquid water at various temperatures.

3.2.2. Flow velocity

Average velocity profiles for all protrusion lengths are presented in Fig.9. We observe that the average velocity for all grooved channels is smaller than in the channel with flat walls and actually it decreases as the protrusion length also decreases. This behavior is also detected in the nanochannel case and is described in detail in Kasiteropoulou et al [6]. Moreover, similar behavior is observed in many previous works performed with different simulation methods [44]. For example, Sofos et al [44] studied the effects of wall roughness on the flow in nanochannels by a molecular dynamics simulation and found that as the rectangular wall cavities become narrower, velocity values inside the cavities decrease and fluid atoms tend to be trapped inside them.

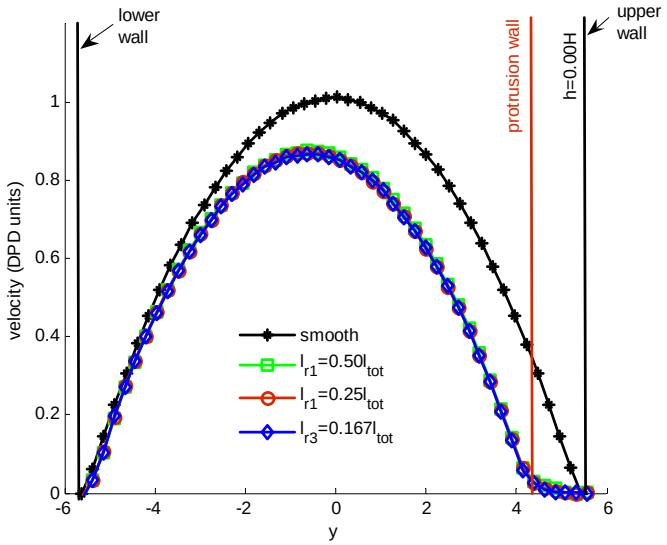

Fig. 9. Average velocity profiles obtained for N_m=2.5x10^6 and $a_{wf} = a_{ff} = a_{ww}$ = 7.5 (parameters kept constant: the cut-off radius r_c = 1.0 and the external driving force F_{ext} = 0.02) for cases a) l_{r1}=0.5l_{tot}, b) l_{r2}=0.25l_{tot}, c) l_{r3}=0.167l_{tot} . Dash-dot lines denote solid wall limits and y is in r_c units.

3.2.3. Isobars

Pressure behaviour also reveals interesting characteristics (Fig.7, 10). Both in the nanochannel case (Fig.7) as well as in the microchannel case (Fig.10), pressure remains constant in the central part of the channel and decreases as we move towards to the walls.

High pressure regions are observed inside the grooves and their magnitude depends on the groove shape (Figs. 10a, 10b, 10c). Smaller protrusion lengths lead to pressure reduction and shorten (across the y-direction) high pressure regions. For case lr_1 (Fig. 10a), the length of the high pressure region inside the cavity is about 2% of the protrusion height, while for cases lr_2 (Fig. 10b) and lr_3 (Fig. 10c) it is 25% and 50% respectively. Pressure profile towards the lower flat wall is not affected by the presence of protrusion elements in the upper wall.

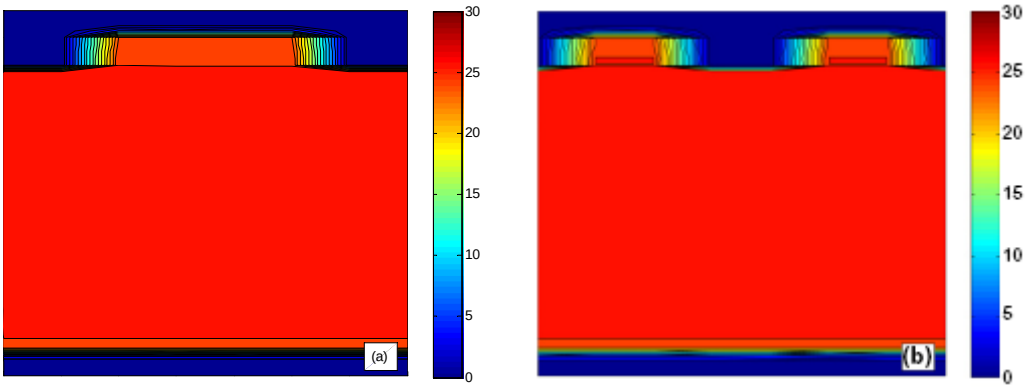

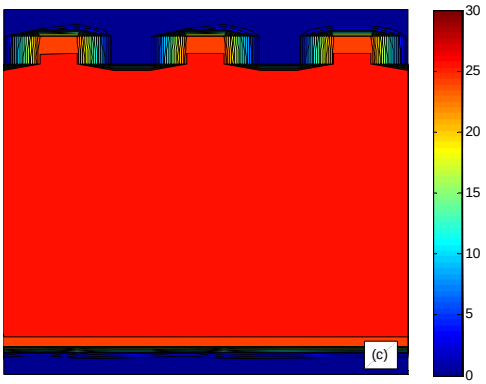

Fig. 10. Isobars obtained for $N_m=2.5x10^6$ and $a_{wf} = a_{ff} = a_{ww} = 7.5$ (parameters kept constant: the cut-off radius $r_c = 1.0\sigma$ and the external driving force $F_{ext} = 0.02$) for cases a) $l_{r1}=0.5l_{tot}$, b) $l_{r2}=0.25l_{tot}$, c) $l_{r3}=0.167l_{tot}$. Dash-dot lines denote solid wall limits and y is in r_c units.

4 CONCLUDING REMARKS

In this paper, we have presented DPD simulations of flow in periodically grooved nano- and microchannels. The rough wall was designed by placing a number of orthogonal protrusions and cavities of equal length in a periodic pattern. Calculations of density, velocity and pressure maps or profiles show clearly that the fluid/wall interaction, the range of interaction of DPD particles, the external driving force and the coarse-graining parameter affect considerably the fluid motion. Number density values in the core of the channel and inside the cavities decreases as the conservative force parameter decreases. The cut-off radius affects density values near the walls and inside the cavities. The value of the external driving force has no significant effect on fluid ordering.

Velocity values in the core of the channel and inside the cavities increases as the conservative force parameter and the external driving force increases and the cut-off radius decreases for all channel cases studied here.

Pressure is strongly affected by the cut-off radius and the conservative force parameter amplitude. For all parameters, as the parameter increases pressure also increases both in the core of the channel and inside the cavities. Inside the cavities high pressure regions are detected and their shape and topology depend on the protrusion length.

Interesting behavior is presented in the microscale channel cases. Fluid particle localization is similar for the nanochannel and the microchannel case, as high density peaks are detected for both cases inside the cavities and near the solid walls. Differences are observed in the core of the channel and in the cavity and protrusion midplanes. In particular, in the nanochannel and the protrusion midplane density is slightly lower than its average value and at cavity is higher, in addition to the microchannel case where at the protrusion midplane it is equal to its average value and at the cavity it is lower. Density peaks inside the cavities reveal trapping of fluid inside the rectangular cavities. This particle trapping affects macroscopic quantities considered here such as velocity and pressure distribution inside and close to the cavities. Velocity reduces systematically and this reduction becomes more pronounced as the protrusion length decreases. For the microchannel, the pressure remains almost constant in the core of the channel and its pattern near and inside the cavities depend on the protrusion shape.

Different materials for the wall and fluid particles, several fluid and wall interface conditions and different fluid types on nano and microchannels with grooves on the upper

wall were investigated. The effect on density, velocity, and pressure distributions were outlined. Although significant progress has been made towards the development and research of grooved channels investigated with different numerical frameworks, the current state of the art does not represent in detail the situation close to the wall in the mesoscale case and remains on the qualitative flow behavior under special circumstances. Future research and development is required to address methods for the near wall region behavior at the mesoscale case and compare their results with other research methods. One has to take into consideration the applied research interest of solid grooved surfaces and their involve in micro/nano electromechanical systems (known as MEMS/NEMS), the cooling of micro and nano devices, the lab-on-chip devices, the drug delivery and the micro and nanofliters. It should be noted that modeling of heat transfer processes requires the implementation of an extension of the DPD method that incorporates the energy transport equation, known as eDPD [43].

REFERENCES

[1] P. Koumoutsakos, Multiscale flow simulations using particles. *Annual Review of Fluid Mechanics,* **37**, 457-487, 2005.

[2] J. Davies, D. Maynes, B.W. Webb, B. Woolford, Laminar flow in a microchannel with superhydrophobic walls exhibiting transverse ribs. *Physics of Fluids*, **18**, 087110-1-11, 2006.

[3] A. Niavarani, N.V. Priezjev, Modelling the combined effect of surface roughness and shear rate on slip flow of simple fluids. *Physical Review E,* **81**, 011606-1-32, 2010.

[4] R. Kamali, A. Kharazmi, Molecular dynamics simulation of surface roughness effects on nanoscale flows. *International Journal of Thermal Sciences,* **50**, 226-232, 2011. doi:10.1016/j.ijthermalsci.2010.05.004

[5] N. Asproulis, D.Drikakis, Surface Roughness Effects in Micro and Nanofluidic Devices. *Journal of Computational and Theoretical Nanoscience*, **7(9)**,1825-1830, 2010.

[6] D. Kasiteropoulou, T. Karakasidis, A. Liakopoulos, A Dissipative Particle Dynamics study of flow in periodically grooved nanochannel. *International Journal for Numerical Methods in Fluid*s, **68(9)**,1156-1172, 2011.

[7] J. Sun, Y.L. He, W.Q. Tao, J.W. Rose, H.S. Wang, Multi-scale study of liquid flow in micro/nanochannels of surface wettability and topology. *Microfluidics and Nanofluidics,* **12**, 991-1008, 2012. DOI 10.1007/s10404-012-0933-7

[8] N.V. Priezjev, Interfacial friction between semiflexible polymers and crystalline surfaces. *The Journal of Chemical Physics*, **136**, 224702-1-10, 2012.

[9] W. Chen, R. Zhang, J. Koplik, Velocity slip on curved surfaces. *Condensed Matter,* **1**, 1-5, 2013. axix.org/pdf/1309.1423v1.

[10] N. Priezjev, Molecular dynamic simulations of oscillatory Couette flows with slip boundary conditions. *Microfluidics and Nanofluidics*, **14**, 225-233, 2013.

[11] F. Sofos, T.E. Karakasidis, A. Liakopoulos, How wall properties control diffusion in grooved nanochannels: a molecular dynamic study. *Heat and Mass Transfer*, **49**, 1081-1088, 2013.

[12] R.A. Sahan, A. Liakopoulos, H. Gunes, Reduced Dynamical Models of Nonisothermal Transitional Grooved-Channel Flow. *Physics of Fluids,* **9**, 551-565, 1997.

[13] A. Liakopoulos, P.H. Blythe, H. Gunes, A reduced dynamical model of convective flows in tall laterally heated cavities. *Proceeding of the Royal Society of London*, **453**, 663-672, 1997.

[14] M. Greiner, R.J. Faulkner, V.T Van, H.M. Tufo, P.F. Fischer, Simulations of Three Dimensional Flow and Augmented Heat Transfer in a Symmetrically Grooved Channel, *Journal of Heat Transfer,* **122**, 653-660, 2000.

[15] Y.M. Chung, P.G. Tucker, D.G. Roychowdhury, Unsteady laminar flow and convective heat transfer in a sharp 180^o bend. *International Journal of Heat and Fluid Flow,* **24**, 67-76, 2003.

[16] Y.M. Chung, P.G. Tucker, K.H. Luo, Large-eddy simulation of complex internal flows, *in Direct and Large-Eddy Simulation IV, Eds. B. Geurts, R. Friedrich, O. Metais*, London, 2001.

[17] T. Adachi, S. Hasegawa, Transition of the Flow in a Symmetric Channel with Periodically Expanded Grooves. *Chemical Engineering Science* , **61**, 2721-2729, 2006.

[18] M. Hahn, D. Drikakis, Large eddy simulation of compressible turbulence using high-resolution methods. *International Journal for Numerical Methods in Fluids*, **47**, 971-977, 2005.

[19] B. Thornber, D. Drikakis, Implicit Large Eddy Simulation of a Deep Cavity Using High-Resolution Methods. *AIAA Journal,* **46(10)**, 2634-2685, 2008.

[20] M. Kalweit, D. Drikakis, Coupling strategies for hybrid molecular-continuum simulation methods, *Procceedings of IMechE Collection, Part C: J. Mechanical Engineering Science*, **222**, 797-806, 2008.

[21] N. Asproulis, M. Kalweit, D. Drikakis, A Hybrid Molecular Continuum Method using Point Wise Coupling. *Advances in Engineering Software*, **46, Issue 1**, 85-92, 2012.

[22] E.E. Keaveny, I.V. Pivkin, M. Maxey, G. Karniadakis, A comparative study between dissipative particle dynamics and molecular dynamics for simple- and complex-geometry flows. *The Journal of Chemical Physics*, **123**, 104107-1-104107-9, 2005.

[23] R.D Groot, P.B. Warren, Dissipative particle dynamics: bridging the gap between atomistic and mesoscopic simulation. *The Journal of Chemical Physics,* **107**, 4423-4435, 1997.

[24] D.A. Fedosov, I.V. Pivkin, G.E. Karniadakis, Velocity limit in DPD simulations of wall-bounded flows. *Journal of Computational Physics,* **227**, 2540-2559, 2008.

[25] P. Espanol, P. Warren, Statistical mechanics of dissipative particle dynamics. *Europhysics Letters,* **30**, 191-196, 1995.

[26] G. Karniadakis, A. Beskok, N. Aluru, *Microflows and Nanoflows: Fundamentals and Simulation*, New York :Springer, 2002.

[27] Y. Trofimov, *Thermodynamic consistency in dissipative particle dynamics*. Technische Universiteit Eindhoven, Ph.D. Thesis, 2003.

[28] P. Nikunen, M. Karttunen, I. Vattulainen, How would you integrate the equations of motion in dissipative particle dynamics simulations?. *Computer Physics Communications,* **, 153**, 407-423, 2003.

[29] I.V. Pivkin, G.E. Karniadakis, A new method to impose no-slip boundary conditions in dissipative particle dynamics. *Journal of Computational Physics,* **207**, 114-128, 2005.

[30] S.J. Plimpton, Fast Parallel Algorithms for Short-Range Molecular Dynamics. *Journal of Computational Physics,* **117**, 1-19, 1995.

[31] D. Kasiteropoulou, T.E. Karakasidis, A. Liakopoulos, Dissipative Particle Dynamics investigation of parameters affecting planar nanochannel flows. *Material Science and Engineering B,* **176(9)**, 1574-1579, 2011.

[32] A. Kumar, Y. Asako, E. Abu-Nada, M. Krafczyk, M. Faghri, From dissipative particle dynamics scales to physical scales: a coarse-graining study for water flow in microchannel. *Microfluidics and Nanofluidics*, **7**, 467-477, 2009.

[33] M. Revenga, I. Zuniga, P. Espanol, Boundary conditions in dissipative particle dynamics. *Computer Physics Communications*, **121–122**, 309-311, 1999.

[34] J.H. Irving, J.G. Kirkwood, The statistical mechanics of transport processes. IV. The equation of hydrodynamics. *The Journal of Chemical Physics*, **18**, 817-830, 1950.
[35] X. Fan, N. Phan-Thien, N. Yong, X. Wu, D. Xu, Microchannel flow of a macromolecular suspension. *Physics of Fluids*, **15 (1)**, 11-21, 2003.
[36] F. Sofos, T.E. Karakasidis, A. Liakopoulos, Surface wettability effects on flow in rough wall nanochannels. *Microfluidics and Nanofluidics,* **12**, 25-31, 2012. DOI 10.1007/s10404-011-0845-y
[37] S.C. Young, Effects of surface roughness and interface wettability on nanoscale flow in a nanochannel. *Microfluidics and Nanofluidics,* **2**, 501-511, 2006.
[38] N.V. Priezjev, Effects of surface roughness on rate-dependent slip in simple fluids. *The Journal of Chemical Physics,* **127**, 144708, 2007.
[39] D. Kasiteropoulou, T. Karakasidis, A. Liakopoulos, Mesoscopic simulation of fluid flow in periodically grooved microchannels. *Computers & Fluids,* **74**, 91-101, 2013.
[40] D. Kasiteropoulou, T. Karakasidis, A. Liakopoulos, Study of fluid flow in grooved micro and nano-channels via dissipative particle dynamic: a tool for desalination membrane design. *Desalination and Water Treatment,* 2016. doi: 10.1080/19443994.2016.1141118
[41] I.V. Pivkin, G. Em. Karniadakis, Controlling density fluctuations in wall-bounded dissipative particle dynamics systems. *Physical Review Letters*, **96**, 206001, 2006. DOI:http://dx.doi.org/10.1103/PhysRevLett.96.206001
[42] T. Werder, J.H. Walther, P. Koumoutsakos, Hybrid atomistic–continuum method for the simulation of dense fluid flows. *Journal of Computational Physics*, **205**, 373–390, 2005.
[43] Z. Li, Y.-H. Tang, H. Lei, B. Caswell, G. Karniadakis, Energy-conserving dissipative particle dynamics with temperature-dependent properties. *Journal of Computational Physics,* **265**, 113–127, 2014.
[44] F.D. Sofos, T.E. Karakasidis, A. Liakopoulos, Effects of wall roughness on flow in nanochannels. Physical Review E, **79**, 026305:1-026305:7, 2009. doi: 10.1103/PhysRevE.79.026305.